Solar photocatalytic degradation of RB5 by ferrite bismuth nanoparticles synthesized via ultrasound

T. Soltani, M.H. Entezari *

Department of Chemistry, Ferdowsi University of Mashhad, 91775 Mashhad, Iran

A B S T R A C T

In this paper, the photocatalytic degradation of Reactive Black 5 (RB5) was investigated with ferrite bismuth synthesized via ultrasound under direct sunlight irradiation. The intensity of absorption peaks of RB5 gradually decreased by increasing the irradiation time and finally vanished in 50 min in acidic medium. The formation of new intermediate was observed in basic medium. The relative concentration of RB5 in solution and on the surface of ferrite bismuth ($BiFeO_3$) nanoparticles was considered during the experiment in acidic and basic media. The effects of various parameters such as amount of catalyst, concentration of dye, and pH of the solution have been studied on the dye degradation. The adsorption isotherm and the kinetic of photocatalytic degradation of RB5 were investigated. The adsorption constants in the dark and in the presence of sunlight irradiation were compared. The photocatalytic degradation mechanism of RB5 has been evaluated through the addition of some scavengers to the solution. In addition, the stability and reusability of the catalyst were examined in this work.

1. Introduction

Sixty to seventy percent of dyes used in the textiles industries contained azo dyes with one or more azo bonds (–N=N–). The intense use of azo dyes is related to their high solubility, stability and color variety and most important its simple dyeing procedure [1]. It is estimated about 15% of the total world production of dyes is lost and is released in the textile effluents during the dyeing process [2]. Some of these dyes not only are toxic, mutagenic [3] and carcinogenic [4] compounds, but also are resistant to aerobic biodegradation [5], and their half-lives under sunlight are greater than 2000 h [6]. These dyes even at low concentration stop the sunlight access to aquatic fauna and flora, and it reduces the photosynthetic action within the ecosystem [7]. Hence, the textile industries are very important source of pollution of the aquatic system.

Lately, there has been considerable attention for the removal of dyes by different methods. There are often used adsorption as a physical method [8], chlorination, ozonation as chemical methods [9] and biodegradation [10]. These removal methods are not effective for a complete degradation and in some cases only provide separation of the dyes without any dye degradation, and creating a secondary waste problem.

Advanced oxidation processes (AOPs) are based on generation of reactive species through illumination of UV or solar light of some active materials. This process can lead to oxidize organic pollutants to inorganic compounds [11]. From the practical point of view, photodegradation of pollutants using semiconductor and solar light is an economical process. Since, the solar energy is an abundant natural energy source, which can be used instead of artificial light sources that is expensive and hazardous.

TiO_2 is widely used for the degradation of many organic compounds under UV irradiation because of its low cost, high stability and high photocatalytic activities [12]. The band-gap energy of TiO_2 is 3.2 eV that can be activated by radiation of UV in the wavelength of 387.5 nm. It is known that only 4–5 percent of solar radiation is UV and this is a limitation for this catalyst which requires UV light for activation.

Nowadays, the perovskite-type $BiFeO_3$ (BFO) has attracted considerable attention due to its narrowing band-gap energy (2.1 eV) [13], high chemical stability [14], and exhibiting a coexistence of simultaneous ferroelectric and magnetic order parameters [15]. In addition to potential electronic and magnetic applications, BFO powders have been used as a new visible-light photocatalyst [16].

Ultrasound has been successfully used for the synthesis of nanocrystalline materials due to its unique effects in recent years [17]. In our lab, the sono-synthesis of semiconductors with core–shell structure was carried out in short time and the product had appropriate adsorbability, and high catalytic activity [18–21]. Great attention has also been paid to the direct use of ultrasound for the degradation of wastewater. But, a complete mineralization of organic pollutants by ultrasonic irradiation alone is difficult. A significant decrease in the concentration of RB5 (94%) was

* Corresponding author. Fax: +98 511 8795457.
E-mail address: moh_entezari@yahoo.com (M.H. Entezari).

observed in our lab in short time under sonication of the solution containing the core–shell nanocomposite. While under similar conditions, the concentration of dye was decreased to 4% under only sonication and 50% under UV light with nanocomposite [22,23].

In this work, the sono-synthesized BFO as a new catalyst was used for the degradation of RB5 as a representative dye pollutant of the textile wastewaters.

2. Experimental

2.1. Chemical and materials

Bismuth nitrate (Bi(NO$_3$)$_3$·5H$_2$O), Iron nitrate (Fe(NO$_3$)$_3$·9H$_2$O), Ethylene glycol (EG) and Ethanol from Merck and RB5 from Dystar Company of Germany have been used without further purification. Isopropanol and sodium fluoride (NaF) from Aldrich, potassium iodide (KI) from Merck were used as scavengers and de-ionized water was used for the sample preparation.

2.2. Catalyst preparation

First, to form a transparent solution, 0.008 mol bismuth nitrate (Bi(NO3)$_3$·5H$_2$O) was sonicated in ethylene glycol for 15 min. During sonication, the temperature of solution was increased from 9 to 35 °C. Without ultrasound, this step was strried for 150 min at 35 °C to reach a transparent solution. Then, stoichiometric proportion of iron nitrate (Fe(NO$_3$)$_3$·9H$_2$O) was added and sonicated for another 15 min to obtain a brownish red sol. It should be mentioned that without sonication, this step lasts 60 min to reach a brownish red sol. Then, the sample was kept in oven at 80 °C for several hours to form a xerogel substance. The obtained powder was calcined at different temperatures (400 and 500 °C, 0.5 h in each temperature), washed with distilled water and absolute alcohol for several times, and dried at 70 °C.

2.3. Characterization and equipment

The crystalline structure of obtained powder was identified by X-ray diffraction (XRD, Phlips PW1800) employing Cu K$_\alpha$ (λ = 1.5406 Å, 2θ = 10–70°). The sizes of the samples were determined with transmission electron microscope (TEM, Leo 912 AB). The light absorption ability of BFO nanoparticles and the absorption spectrum of RB5 were analyzed by UV–vis spectra (unico2600). The sample for UV–vis analysis was dispersed in ethanol to form a homogeneous suspension by sonicating for 30 min.

The point of zero charge (pzc) of the nanoparticles was determined by plotting the final pH versus the initial pH [24].

The ultrasonic irradiation operating at 20 kHz (Branson Digital Sonifier, W-450 D, output acoustic power 41 W (amplitude 75%), horn with 1.9 cm diameter) was used for the synthesis of nanoparticles in a Rosset cell. The temperature was controlled by a circulating bath. The Bransonic digital ultrasonic bath (Model 8510) working at 40 kHz was used for the preparation of sample for UV–vis analysis.

2.4. Sunlight irradiation

The Pyrex glass vessel containing 100 mL RB5 (25 mg/L) and appropriate quantity of photocatalyst was magnetically stirred on the window ledge under direct solar radiation. Several stirrers were used simultaneously in equal rates of stirring during the predetermined time intervals. The irradiation by sunlight was carried out in consecutive sunny days in July 2012 between 11.30 am and 2.00 pm (GPS coordination: N = 36°18′41.6″, E = 59°31′54.2″). The

temperature of the solution was between 28 and 32 °C. Before starting with sunlight irradiation, the suspensions were magnetically stirred in the dark place for 45 min to attain adsorption–desorption equilibrium between the dye and photocatalyst. Then, in appropriate interval times, about 5 mL of suspensions was withdrawn and after separation of catalyst from the solution with an external magnetic field, the concentration of RB5 was measured using UV–vis at 600 nm and 620 nm in acidic and basic media, respectively. This measurement was done for both samples in the dark and under sunlight. The absorption was converted to the concentration through the standard curve of RB5 (Supporting information Fig. S1(a): acidic medium, (b): basic medium).

Experiments under different pH were also carried out to reveal the role of pH on the photocatalytic activity of BFO nanoparticles. The pH values were adjusted by adding HCl or NaOH solution.

3. Results and discussion

3.1. Characterization of the catalyst

Fig. 1 shows the XRD pattern of BFO nanoparticles synthesized via ultrasound under mild conditions. The peaks in the XRD pattern were corresponded to the rhombohedral structure of BFO with R3c space group (JCPDS no: 71-2494), and the calculated lattice parameters a = b = 5.5774 Å and c = 13.8667 Å. No additional peaks related to the impurity were observed in the XRD pattern. The crystalline size of the sample based on Debye–Scherrer formula was about 50 nm according to the (0 1 2) diffraction peak. Ultrasound can provide high mixing of the starting materials that is appropriate for preparation of sample with high degree of purity, crystalline structure, and small particle size in a short time.

Fig. 2(a) shows the TEM image of pure BFO nanoparticles. The particles are roughly spherical with an average size of about 60–80 nm based on Fig. 2(b).

3.2. UV–vis analysis

UV–vis spectrum of the nanoparticles synthesized via ultrasound is shown in Fig 3. The nanocrystals can absorb considerable amounts of visible light that is appropriate as visible-light driven photocatalysts. The inset of Fig. 3 shows the calculation of the band-gap energy by using Tauc's equation [25], $(ah\nu)^n = B(h\nu - E_g)$. Where a, h, v, E$_g$ and B are absorption coefficient, Planck constant, light frequency, band gap energy, and a constant, respectively. The
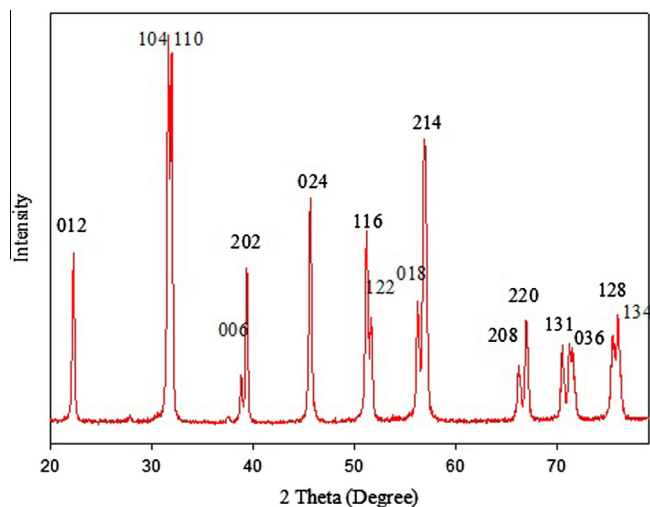

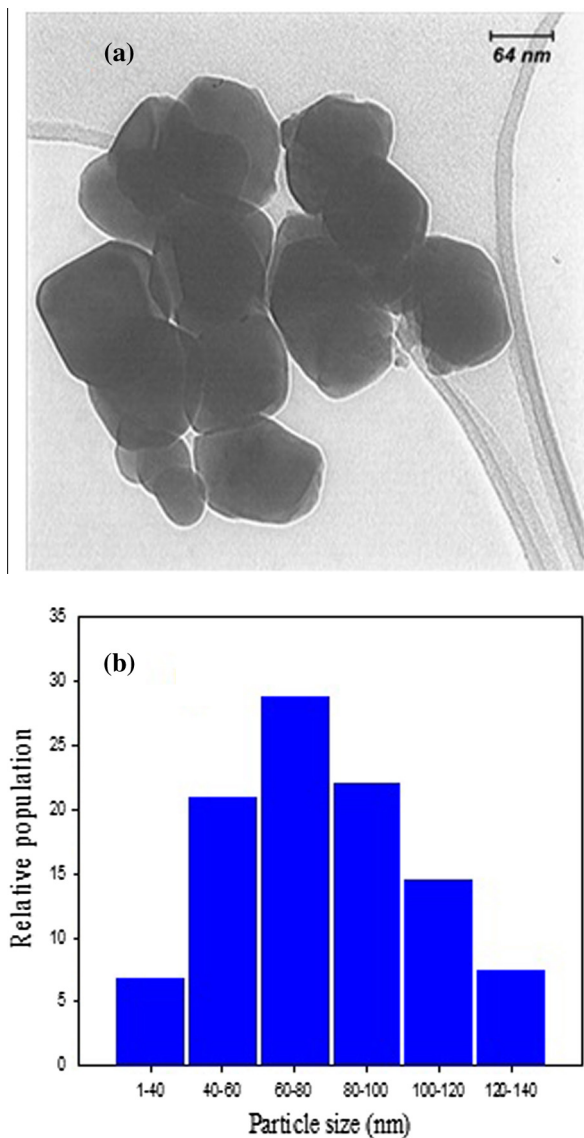**Fig. 1.** XRD pattern of BFO nanoparticles synthesized by ultrasonic method.

value of n for BFO is 2 which indicates a direct band gap. As shown in the inset of Fig. 3, the corresponding band gap energy of the sample can be estimated by extrapolating the linear portion of $(ah\nu)^2$ against hν plot to the point a = 0.

The band gap energy is estimated about 2.07 eV in accordance with the previous reports [26] that is appropriate for the degradation of organic pollutants in the visible range.

3.3. Method of photocatalyst synthesis

For comparison, two samples were synthesized via sol–gel and ultrasonic methods. The results show in Fig. 4. The degradation of RB5 by nanoparticles synthesized via ultrasound was more effective than of the corresponding sol–gel nanoparticles in both acidic and basic media.

The average crystallite size for the sample prepared via sol–gel method was 82.0 nm based on Debye–Scherrer formula. The nanoparticles synthesized with ultrasound exhibited smaller crystallite size (about 50 nm) than the nanoparticles synthesized via sol–gel method in stricter conditions. The higher photocatalytic activities of the sample synthesized via ultrasound could be attributed to its smaller crystallite size and higher surface area. This means that the number of sorption sites and radical species increase for the nanoparticles synthesized via ultrasound. In addition, the high-temperature and high pressure produced during the asymmetric cavitations provide a favorable environment for the growth of nanocrystals [17].

The results show that the nanoparticles synthesized via ultrasound in both acidic and basic media exhibited a higher photocatalytic activity than the nanoparticles synthesized via sol–gel method. Therefore, the whole experiments were performed with the sample synthesized by ultrasound.

3.4. Effect of catalyst loading

The amount of catalyst is one of the main parameter for the degradation studies. In order to study the effect of dosage on the photodegradation efficiency, different values in the range of 0.25–1.00 g/L were applied in constant dye concentration (25 mg/L) and the results are shown in Fig. 5. Before illumination, the suspensions were stirred in dark for 45 min to reach an adsorption–desorption equilibrium between the photocatalyst and RB5 (Fig. 5(a)). The results in dark with 0.25 g/L of catalyst showed that

Fig. 2. (a) TEM and (b) particle size distribution of BFO nanoparticles synthesized by ultrasonic method.

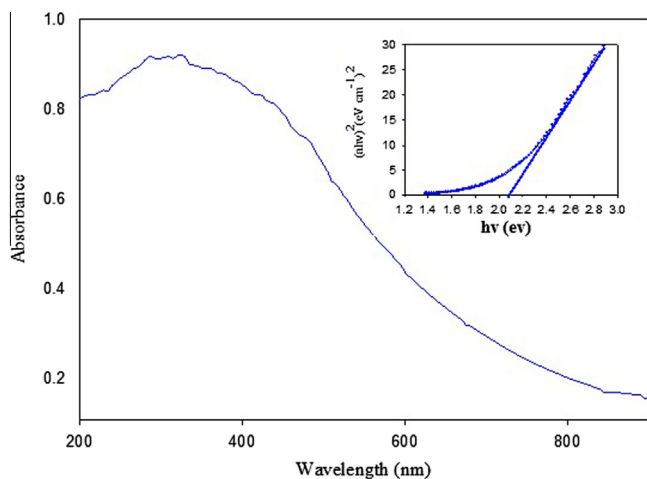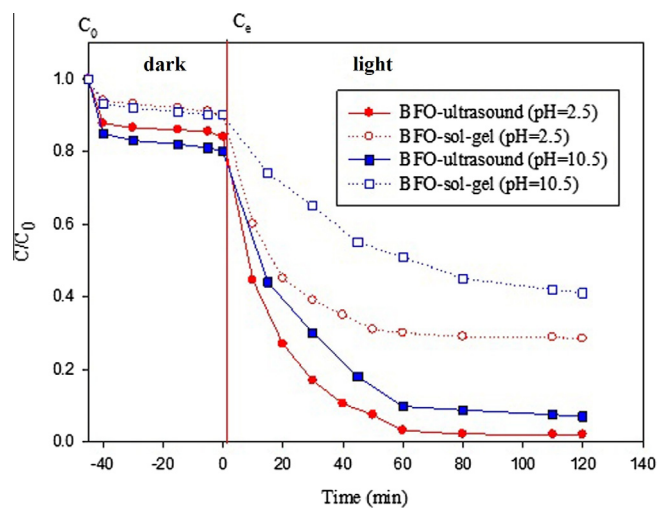**Fig. 3.** UV–vis spectrum of BFO nanoparticles, the inset shows the calculation of the band gap energy.

Fig. 4. photodegradation of RB5 on BFO nanoparticles synthesized by ultrasound and sol–gel methods (c_0 = 25 mg/L, pH = 2.5, dosage of catalyst = 0.5 g/L, temperature = 28–32 °C).
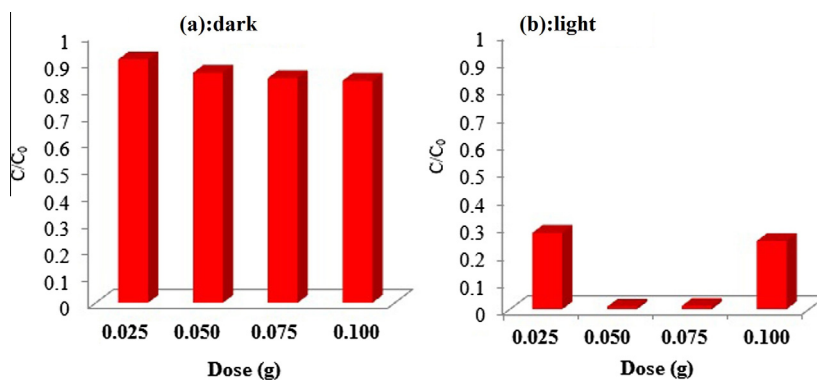
Fig. 5. Effect of catalyst loading on the (a) adsorption efficiency and (b) degradation efficiency of RB5 (c_0 = 25 mg/L, pH = 2.5, time of irradiation = 50 min, temperature==28–32 °C).

only less than 8% RB5 was adsorbed by catalyst after 45 min. But, under light irradiation about 70% RB5 was degraded. With increasing the dosage value to 0.50 g/L, approximately 15% RB5 was adsorbed by catalyst in dark and 99% RB5 was degraded after 50 min. The similar result was obtained with 0.75 g/L of catalyst. By increasing the amount of catalyst to 1.00 g/L, the total active site on the surface of catalyst increases but, there will be a decrease in penetration of sun light irradiation due to an increase in turbidity of the suspension [27,28]. Therefore, it can be concluded that higher dosage of catalyst may not be useful because of aggregation and reduction of the irradiation field due to light scattering.

The results confirmed that the lowest degradation was obtained with 0.25 g/L of BFO nanoparticles and the highest was obtained with 0.50 g/L. Hence, the whole experiments were continued with 0.50 g/L of the catalyst.

3.5. Effect of pH

One of the most important parameter that influences the photocatalytic degradation is pH. The effect of initial pH on the photocatalytic degradation of RB5 as a function of time is shown in Fig. 6. The experiments were conducted in various initial pH values ranging from 2.5 to 10.5 in a constant dye concentration (25 mg/L), catalyst loading (0.50 g/L) and 50 min of sunlight irradiation. The increase and decrease of initial pH solution from natural pH (5.5, with 24% degradation), increases the dye degradation to 91% (pH = 10.5) and 99% (pH = 2.5). The surface charge of BFO nanoparticles changes with change of pH solution. According to the other
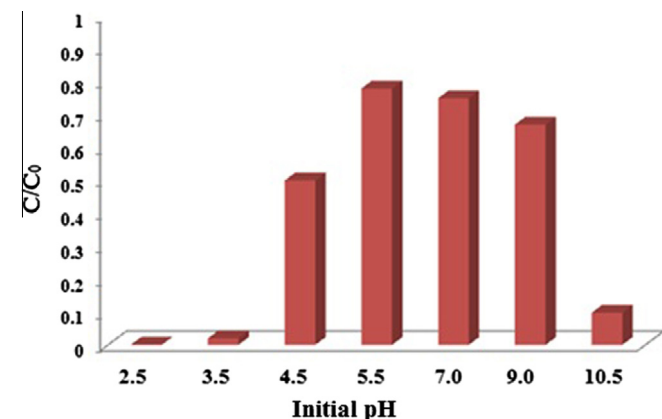
results, positive holes are responsible as the major oxidation species at low pH, whereas hydroxyl radicals are considered as the predominant species in neutral or high pH [29].

3.6. Photocatalytic degradation in acidic and basic media

The UV–vis spectrum of RB5 (Fig. 7) contains five absorption peaks. The essential peak is in visible region (600 nm) with a shoulder around 500 nm and others are in ultraviolet range (229, 254, 312, and 391 nm). The absorption peak at 600 nm can be assigned to a chromophore containing a long conjugated π-system linked by two azo groups [30]. The absorption peaks at 312 and 254 nm can be attributed to the naphthalene and benzene components, respectively (Supporting information Fig. S2) [31]. These peaks are related to the transition of electrons from π bonding to the π^* antibonding orbital. In addition, two sources of nitrogen including azo and amine groups linked to a naphthalene ring present in RB5.

Fig. 7 shows the UV–vis spectra of RB5 in aqueous solution in the presence of catalyst at different interval times (pH = 2.5). The spectra reveal that no new intermediates or products formed. The absorption peaks are decreased in intensity with increasing irradiation time, vanishing almost completely within 50 min. The rapid disappearance of the 600 nm absorption band suggests that the chromophore structure responsible for the characteristic color of the azo dye is breaking down. In addition, opening of benzene or naphthalene rings occurs as speedy of the decolonization that is due to the bond-breaking between aromatic rings and azo group. After 50 min (Fig. 7), the colorless compounds without naphthalene and benzene groups formed in the reaction medium.

Inset of Fig. 7 shows the relative concentration of RB5 in solution and on the surface of photocatalyst during the experiments. According to the desorption test, after reaching equilibrium in dark (45 min), approximately less than 10% of the dye was adsorbed and 90% was remained in the solution. In the presence of light, the concentration of dye on the surface and in the solution was decreased differently with irradiation time. The degradation can take place on the surface or in the bulk of solution. After 50 min of sunlight irradiation, the relative concentration of dye in solution and on the surface is negligible and most of them were degraded.

In basic medium (Fig. 8), the UV–vis spectrum of RB5 is partly different from acidic medium and generally exhibits three main peaks at wavelengths of 620, 312, and 254 nm. As shown in Fig. 8, with increasing the time of irradiation, new intermediates formed in the visible and ultraviolet regions that can be related to the separation of sulfone, sulfonate and amine groups from the dye molecule. In addition, the inset of Fig. 8 shows the relative concentration of dye in solution and on the surface of catalyst during the sunlight irradiation.
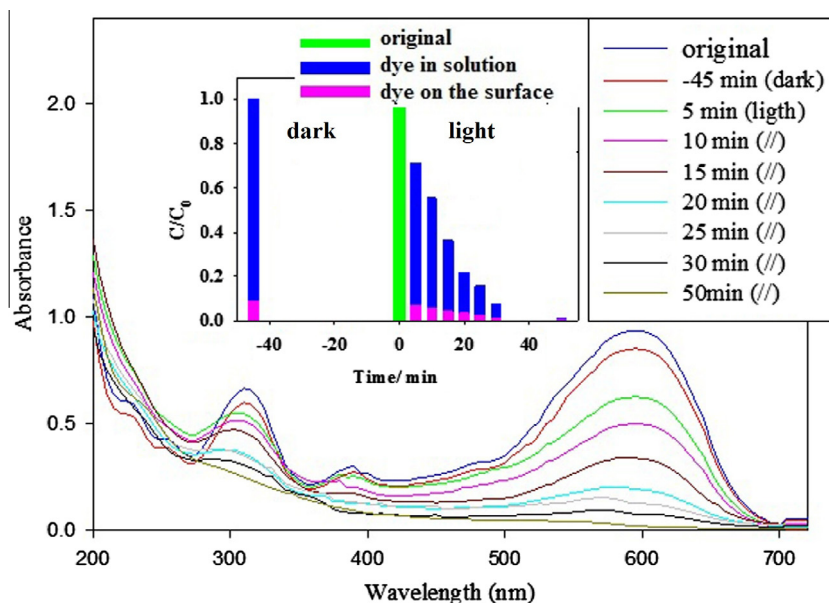

Fig. 6. Degradation of RB5 at different initial pH (c_0 = 25 mg/L, time of irradiation = 50 min, temperature = 28–32 °C).

Fig. 7. UV–vis spectra of RB5 solution at different contact times with BFO nanoparticles, the inset is the relative concentration of RB5 in solution and on the surface of BFO nanoparticles (pH = 2.5, dosage of catalyst = 0.5 g/L, temperature = 28–32 °C).

Fig. 8. UV–vis spectra of RB5 solution at different contact times with BFO nanoparticles, the inset is the relative concentration of RB5 in solution and on the surface of BFO nanoparticles (pH = 2.5, dosage of catalyst = 0.5 g/L, temperature = 28–32 °C).
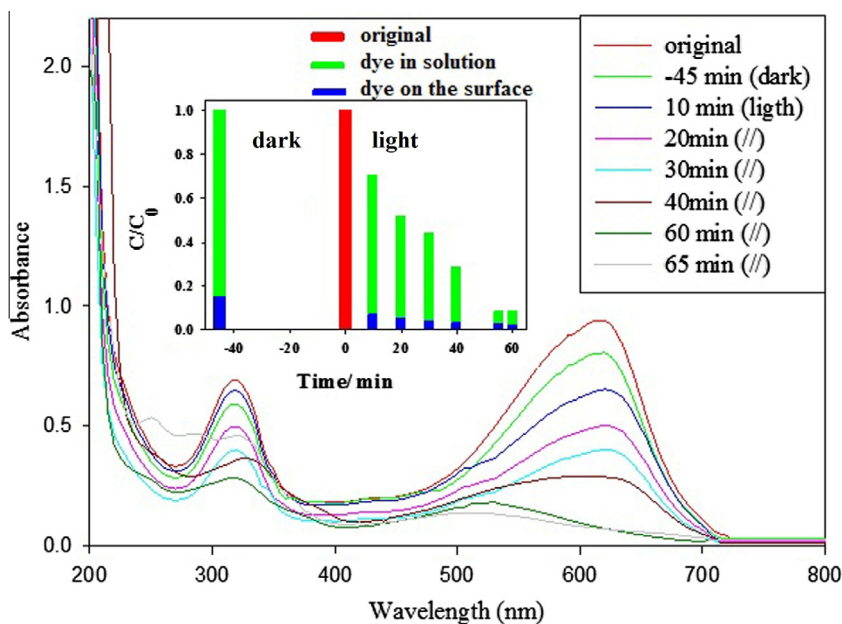
The photolysis process was not observed in acidic medium under applied experimental conditions. Therefore, the decrease of absorption peaks in UV–vis region in acidic medium was due to photocatalytic process. But, in basic media, about 10% of degradation was related to photolysis and the remaining was belong to photocatalytic degradation.

3.7. pH evolution during the RB5 degradation

Fig. 9 shows a fast decrease of initial pH from 10.5 to 9.2 in basic medium after 10 min of irradiation. It decays further to 8.8 with increasing the time of irradiation to 60 min. Some intermediates may be in the form of organic acids that could be the reason for

the decrease of pH [32]. It was also reported the production of nitrate and sulfate ions from sulfone, sulfonate and amine groups of RB5 [33].

$$C_{26}H_{21}N_5O_{19}S_6Na_438O_2 + UV/TiO_2 \rightarrow 26CO_2 + 4H_2O + 4NaNO_3 + HNO_3 + 6H_2SO_4$$
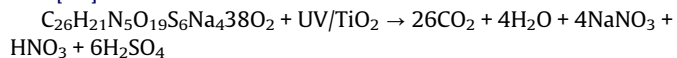
Furthermore, in basic medium, the color changed from dark blue to orange. But, in acidic medium, the initial pH was constant and the color was changed from dark blue to colorless solution.

3.8. Adsorption isotherm

The adsorption of organic molecules on the surface of catalyst plays an important role in the photocatalytic reactions. Thus, it is
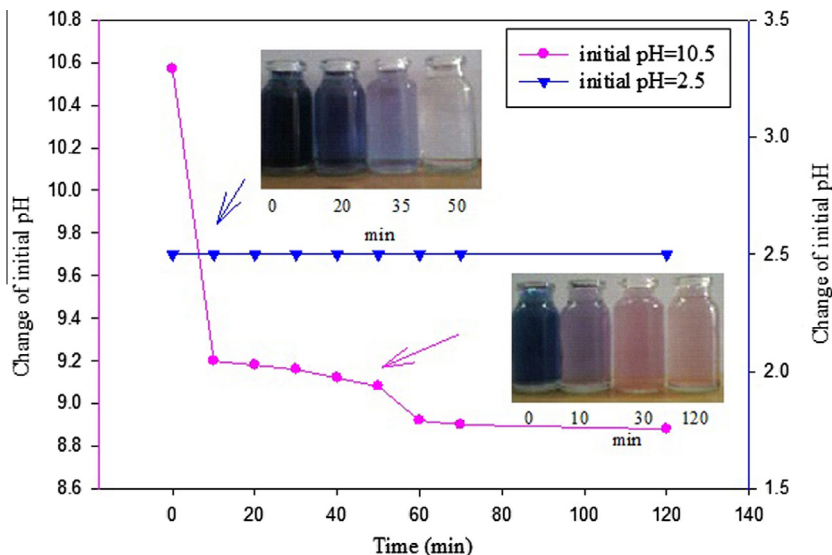
Fig. 9. Change of initial pH versus time.

important to determine the isotherm of adsorption using various concentrations of RB5 in a dark place at pH 2.5. The point of zero charge of BFO is 7.0. Therefore, in acidic medium, the surface of BFO is mainly positive that is appropriate for the adsorption of RB5 by the sulfonate, sulfoxide or sulfone groups. As it is shown in Fig. S3 (information supporting), by increasing the concentration, the amount of RB5 adsorbed on BFO nanoparticles increases before reaching a plateau.

The linear form of the Langmuir model [34] is represented by Eq. (1):

$$\frac{C_e}{q_e} = \left(\frac{1}{q_m K_{ads}}\right) + \left(\frac{1}{q_m}\right) C_e \qquad (1)$$

where q_e (mg/g), c_e (mg/L), K_{ads} (L/mg) and q_m (mg/g) are the amount of dye adsorbed on the photocatalyst at equilibrium, the dye concentration in solution at equilibrium, the Langmuir adsorption constant, and the maximum amount of dye adsorbed on the photocatalyst, respectively. The calculated values of the Langmuir parameters from Fig. 10 are K_{ads} = 0.085 L/mg and q_m = 9.65 mg/g, respectively.
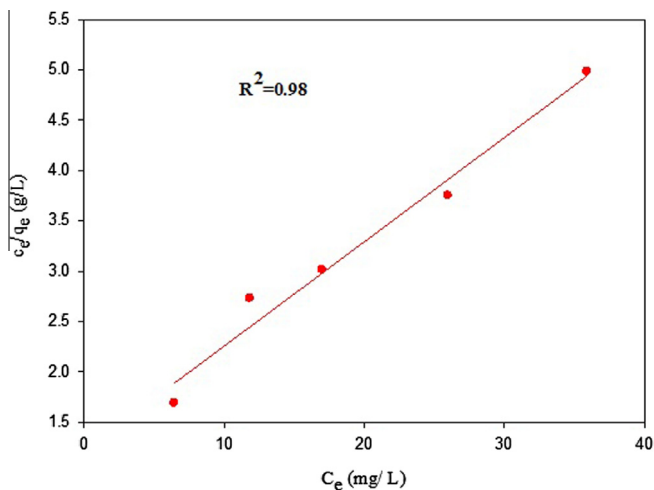

Fig. 10. Langmuir model.

3.9. Kinetics of photocatalytic degradation

The dye concentration is a very important parameter in wastewater treatment. The effect of various initial concentrations of RB5 from 8.5 to 40.0 mg/L has been investigated by the photocatalytic degradation in acidic pH (2.5) and the results are shown in Fig. 11(a). It was found that the increase of concentration decreased the removal rate of RB5. As shown in Fig. 11(b), with increasing the concentration of dye, the maximum amount of adsorption increased and more time is required for compete degradation under sunlight irradiation. In addition, at high concentrations, solar light may be absorbed by the dye rather than by the BFO nanoparticles that may reduce its catalytic efficiency in short time [35].

The photocatalytic degradation of RB5 obeys the pseudo-first-order kinetics in terms of modified Langmuir- Hinshelwood (L-H) model.

$$r = -\frac{dc}{dt} = \frac{k_r K_{LH} C}{1 + K_{LH} C} \qquad (2)$$

In this equation, r (mg/L min), k_r (mg/L min), K_{LH} (L/mg), c (mg/L) and t (min) are the reaction rate, reaction rate constant, adsorption constant, reactant concentration and time of illumination [36], respectively. When c is very small, Eq. (2) can be written in form of Eq. (3).

$$r = -\frac{dc}{dt} = k_r K_{LH} C = kc \qquad (3)$$

where, k (min^{-1}) is the pseudo-first-order rate constant.

In the photocatalytic process, the dye adsorbs onto the BFO surface and reaches equilibrium of adsorption–desorption after 45 min. Then, the equilibrium concentration of the dye solution was used as the initial dye concentration for the kinetic analysis (c_0). Integration of Eq. (3) with the limit of c = c_0 at t = 0 and c = c_t at time t gives Eq (4).

$$\ln \frac{C}{C_0} = -kt \qquad (4)$$

According to Eq. (4), the plot of ln (c/c0) versus t for all concentrations is linear, and the value of k_{app} can be obtained directly via its slope (Fig. 11(c)). It is clear that the initial concentration of RB5
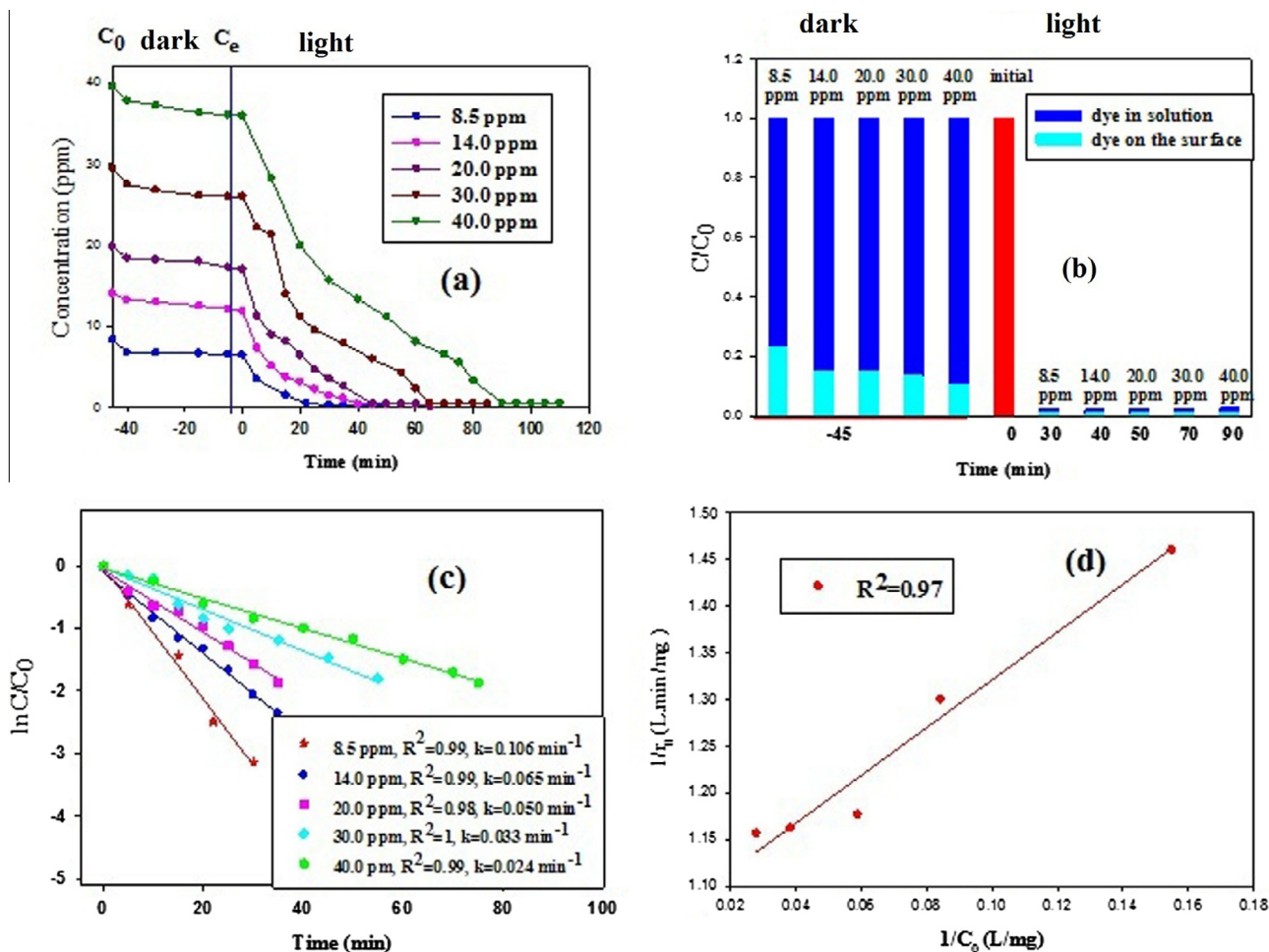
Fig. 11. (a) Effect of initial dye concentration on the degradation of RB5, (b) relative concentration of dye in solution and on the surface, (c) kinetics of photocatalytic degradation of RB5 and (d) kinetic plot of the photocatalytic degradation of RB5 based on L–H equation (pH = 2.5, dosage of catalyst = 0.5 g/L, temperature = 28–32 °C).

has a significant effect on the degradation rates. When the initial concentration is lower, the rate constant of degradation is higher. In another word, the initial degradation rate of the dye increases with increasing the dye concentration and finally reaches a plateau at higher concentrations (Supporting information Fig. S4).

Also, Eq. (2) can be modified as Eq. (5).

$$\frac{1}{r} = \frac{1}{k_r K_{LH} C} + \frac{1}{k_r} \tag{5}$$

The applicability of L–H equation for the degradation has been confirmed by the linear plot obtained by plotting the reciprocal of initial rate ($1/r_0$) against reciprocal of initial concentration ($1/C_0$) as shown in Fig. 11(d).

The K_{LH} = 0.416 L/mg and k_r = 0.936 mg/L min were calculated from the slope and the intercept of straight line (R^2 = 0.97). The value of the adsorption constant determined in the dark using Langmuir model was 0.085 L/mg and the one obtained under sunlight irradiation was 0.416 L/mg. K_{ads} from Langmuir isotherm is smaller than K_{LH} obtained from photocatalytic degradation. Similar results were reported by others [37] and various hypotheses have been suggested for this behavior. The suggestions are as following: (i) the reactions can take place at the surface and in the bulk solution [38], (ii) the solar illumination can change electronic properties of BFO [39], (iii) the heat generated during recombination reactions of active species (electron/hole or radical) can modify the equilibrium of pohotocatalyst at the surface [40].

3.10. Visible light driven degradation mechanism

Some experiments were designed to determine the mechanism of degradation in acidic medium. Before irradiation, the experiments were performed in dark place for 45 min. One experiment was carried out in an aqueous RB5 solution without photocatalyst. The result showedthat the relative concentration of dye did not change with increasing the irradiation time. It means, the dye was stable versus light irradiation without photocatalyst. Then, different scavengers were used to determine the mechanism of degradation, as shown in Fig. 12.

Iodide ion is a scavenger with redox potential of 1.3 V for the couple I·/I⁻, could react with h_{vb+} and OH· [41] and consumes the oxidizing species available at the surface of the catalyst. When 20 mM KI was used, the degradation was strongly inhibited as shown in Fig. 12. This confirms the degradation was mainly proceeded by direct interaction of RB5 with h_{vb}.or OH·. By adding 20 mM isopropanol as a scavenger of the hydroxyl radicals, the degradation of RB5 decreased slightly due to low generation of OH· in the medium.

The results obtained by adding 20 mM NaF were similar to the addition of isopropanol. Since the redox potential of the couple F·/ F⁻ is about 3.6 V, F⁻ is very stable against oxidation even by h_{vb+} [42]. Furthermore, the concentration of surface hydroxyl groups on the BFO nanoparticles can be controlled by adopting fluoride exchange [43]. Based on Fig. 12, by adding 20 mM NaF, the degra-
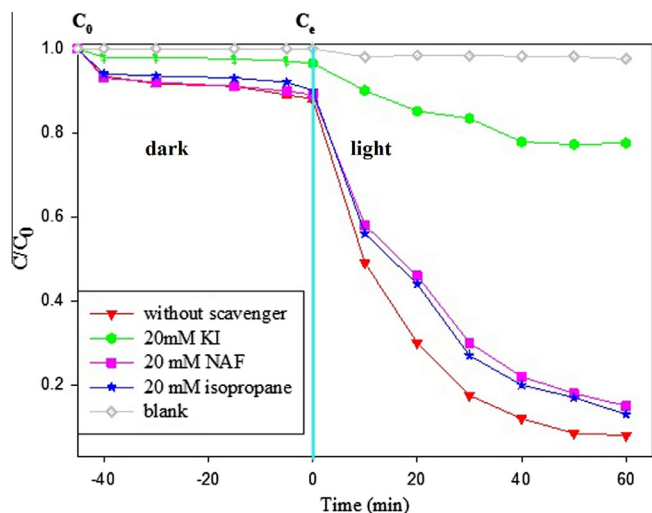
Fig. 12. Effect of different scavengers on the degradation efficiency of RB5 (pH = 2.5, dosage of catalyst = 0.5 g/L, temperature = 28–32 °C).

Fig. 13. Reusability of the catalyst in successive cycles in acidic pH (2.5) (c_0 = 25 mg/L, time of irradiation = 50 min).

dation of RB5 was inhibited slightly. This might be explained by the formation of OH· from OH⁻ groups of RB5 that inhibited through the replacement of the hydroxyl groups on the surface of the catalyst by fluoride ion. This behavior could be attributed to the position of valance band potentials of BFO at the point of zero charge (pH_{zpc}) that can be calculated by the following empirical equation [44].

$$E_{VB} = X − E^e + 0.5E_g \qquad (6)$$

In this equation, E_{VB}, is the VB edge potential, X is the electronegativity of the semiconductor that defined as the geometric mean of the absolute electronegativity of the constituent atoms. Herein, the arithmetic mean of the atomic electron affinity and the first ionization energy are defined instead of the common-defined term [45]. E^e is the energy of free electrons on the hydrogen scale (∼4.5 eV), E_g is the band gap energy of the semiconductor. Then, the E_{CB} can be determined by $E_{CB} = E_{VB} − E_g$. Butler and Ginley [46] calculated band potentials for several oxide semiconductors using this method and the results showed that the predicted values with this method were in good agreement with the measured flat band potentials [47].

The valance band of BFO (2.575 V) is lower than the standard redox potential of OH·/H₂O (2.7 V vs NHE) but, higher than the standard redox potential of OH·/OH⁻ (2.3 V vs NHE) [48]. It means the photogenerated hole can not oxidize the H₂O to form HO· but, it can oxidize the OH⁻ groups of RB5 to OH·.

3.11. Stability and reusability of the catalyst

Estimating the stability and reusability of the catalyst is necessary for the practical applications. To investigate the reusability of BFO nanoparticles, the photocatalytic degradation experiment was repeated several times in acidic medium (pH = 2.5). In each cycle, the suspension was magnetically stirred for 50 min in the presence of sunlight irradiation. Then, the suspension was separated from the solution by an external magnetic field and again, 100 mL of original dye solution was added to the separated solid phase. This experiment was repeated six times (Fig. 13). The results showed a slight decrease in degradation efficiency in successive cycles and the degradation can be completed in longer times. In addition, the BFO nanoparticles were very stable during the applied cycles.
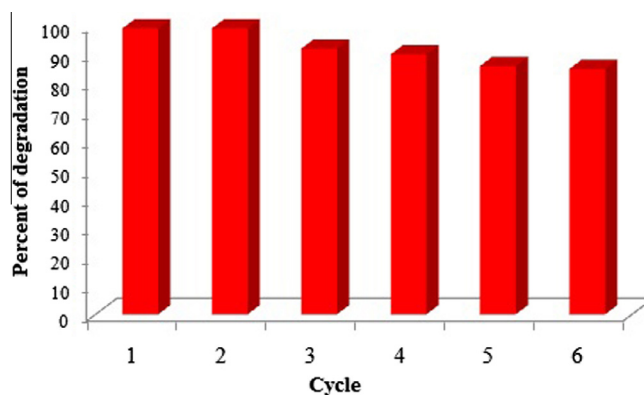
4. Conclusion

The RB5 was successfully degraded by BFO nanoparticles synthesized via ultrasound under sunlight irradiation. The dye was resistant in direct photolysis and the BFO nanoparticles exhibited a higher photocatalytic activity in acidic and basic medium rather than its natural medium. In addition, the sample synthesized via ultrasound showed a higher photocatalytic activity than the sample synthesized via sol–gel method. The degradation of the dye followed a pseudo-first order kinetic according to the Langmuir–Hinshelwood model. K_{ads} obtained from Langmuir isotherm in dark and K_{LH} obtained from the photocatalytic degradation of the dye in the presence of sun light irradiation were compared. After 50 min of sunlight irradiation, the relative concentration of dye in solution and on the surface is negligible. The synthesized photocatalyst was stable and reusable under visible light irradiation in several cycles. The cleavage of the chromophore structure, naphthalene and benzene rings were mainly carried out through the hole and OH· produced during the process.

Appendix A. Supplementary data

Supplementary data associated with this article can be found, in the online version, at http://dx.doi.org/10.1016/j.ultsonch.2013.01.012.

References

[1] N.M. Mahmoodi, M. Arami, Bulk phase degradation of acid red 14 by nanophotocatalysis using immobilized titanium (VI) oxide nanoparticles, J. Photochem. Photobiol. A: Chem. 182 (2006) 60–66.
[2] A. Houas, H. Lachheb, M. Ksibi, E. Elaloui, C. Guillard, J.M. Herrmann, Photocatalytic degradation pathway of methylene blue in water, Appl. Catal. B: Environ. 31 (2001) 145–157.
[3] K.T. Chung, S.E.J. Stevens, C.E. Cerniglia, The reduction of azo dyes by the intestinal microflora, Crit. Rev. Microbiol. 18 (1992) 175–197.
[4] J. Li, P.L. Bishop, Adsorption and biodegradation of azo dye in biofilm processes, Water Sci. Technol. 49 (2004) 237–245.
[5] U. Pagga, D. Brown, The degradation of dyestuffs. II. Behavior of dyestuffs in aerobic biodegradation tests, Chemosphere 15 (1986) 479–491.
[6] N.H. Ince, D.T. Gonenc, Treatability of textile azo dye by UV/H₂O₂, Environ. Technol. 18 (1997) 179–185.
[7] A.G.S. Prado, J.D. Torres, E.A. Faria, S.C.L. Dias, Comparative adsorption studies of indigo carmine dye on chitin and chitosan, J. Colloid Interface Sci. 277 (2004) 43–47.

[8] E.N. El Qada, S.J. Allen, G.M. Walker, Adsorption of basic dyes from aqueous solution onto activated carbons, Chem. Eng. J. 135 (2008) 174–184.

[9] Y.M. Slokar, A.M. Le Marechal, Methods of decoloration of textile wastewaters, Dyes Pigm. 37 (1998) 335–356.

[10] A.T. More, A. Vira, S. Fogel, Biodegradation of trans-1,2-dichloroethyllene by methane utilizing bacteria in an aquifer simulator, Environ. Sci. Technol. 23 (1989) 403–406.

[11] R. Aplin, T.D. Waite, Comparison of three advanced oxidation processes for degradation of textile dyes, Water Sci. Technol. 42 (2000) 345–354.

[12] A.B. Prevot, C. Baiocchi, M.C. Brussino, E. Pramauro, P. Savarino, V. Augugliaro, G. Marci, L. Palmisano, Photocatalytic degradation of acid blue 80 in aqueous solutions containing TiO$_2$ suspensions, Environ. Sci. Technol. 35 (2001) 971–976.

[13] X.Y. Chen, T. Yu, F. Gao, H.T. Zhang, L.F. Liu, Y.M. Wang, Z.S. Li, Z.G. Zou, J.-M. Liu, Application of weak ferromagnetic BiFeO$_3$ films as the photoelectrode material under visible-light irradiation, Appl. Phys. Lett. 91 (2007) 022114–022117.

[14] Z.F. Bian, Y.N. Huo, Y. Zhang, J. Zhu, Y.F. Lu, H.X. Li, Aerosol-spay assisted assembly of Bi$_2$Ti$_2$O$_7$ crystals in uniform porous microspheres with enhanced photocatalytic activity, Appl. Catal. B 91 (2009) 247–253.

[15] T. Choi, S. Lee, Y.J. Choi, V. Kiryukhin, S.W. Cheong, Switchable ferroelectric diode and photovoltaic effect in BiFeO$_3$, Science 324 (2009) 63–66.

[16] J. Luo, P.A. Maggard, Hydrothermal synthesis and photocatalytic activities of SrTiO$_3$ coated Fe$_2$O$_3$ and BiFeO$_3$, Adv. Mater. 18 (2006) 514–517.

[17] K.S. Suslick, S.B. Choe, A.A. Cichowlas, M.W. Grinstaff, Sonochemical synthesis of amorphous. Iron, Nature 353 (1991) 414–416.

[18] M.H. Entezari, N. Ghows, Micro-emulsion under ultrasound facilitates the fast synthesis of quantum dots of CdS at low temperature, Ultrason. Sonochem. 18 (2011) 127–134.

[19] N. Ghows, M.H. Entezari, Ultrasound with low intensity assisted the synthesis of nanocrystalline TiO$_2$ without calcinations, Ultrason. Sonochem. 17 (2010) 878–883.

[20] N. Ghows, M.H. Entezari, A novel method for the synthesis of CdS nano-particles without surfactant, Ultrason. Sonochem. 18 (2011) 269–275.

[21] N. Ghows, M.H. Entezari, Fast and easy synthesis of core–shell nanocrystal (CdS/TiO$_2$) at low temperature by micro-emulsion under ultrasound, Ultrason. Sonochem. 18 (2011) 629–634.

[22] N. Ghows, M.H. Entezari, Exceptional catalytic efficiency in mineralization of the reactive textile azo dye (RB5) by a combination of ultrasound and coreshell nanoparticles (CdS/TiO$_2$), J. Hazard. Mater. 195 (2011) 132–138.

[23] N. Ghows, M.H. Entezari, Kinetic investigation on sono-degradation of Reactive Black 5 with core–shell Nanocrystal, Ultrason. Sonochem. 20 (2013) 386–394.

[24] S.M. Nomanbhay, K. Palanisamy, Removal of heavy metal from industrial wastewater using chitosan coated oil palm shell charcoal, Electron. J. Biotechnol. 8 (2005) 43–53.

[25] D.A. Chang, P. Lin, T.Y. Tseng, Optical properties of ZrTiO$_4$ films grown by radio-frequency magnetron sputtering, J. Appl. Phys. 77 (1995) 4445–4451.

[26] Y.N. Huo, Y. Jin, Y. Zhang, Citric acid assisted solvothermal synthesis of BiFeO$_3$ microspheres with high visible-light photocatalytic activity, J. Mol. Catal. A: Chem. 331 (2010) 15–20.

[27] S. Ahmed, M.G. Rasul, R. Brown, M.A. Hashib, Influence of parameters on the heterogeneous photocatalytic degradation of pesticides and phenolic contaminants in wastewater, J. Environ. Manage. 92 (2011) 311–330.

[28] N. Daneshvar, D. Salari, A.R. Khataee, Photocatalytic degradation of azo dye acid red 14 in water: investigation of the effect of operational parameters, J. Photochem. Photobiol. A: Chem. 157 (2003) 111–116.

[29] V.K. Gupta, Suhas, Application of low-cost adsorbents for dye removal-a review, J. Environ. Manage. 90 (2009) 2313–2342.

[30] M.S. Lucas, J.A. Peres, Decolorization of the azo dye Reactive Black 5 by Fenton and photo-Fenton oxidation, Dyes Pigm. 71 (2006) 236–244.

[31] I. Gultekin, N.H. Ince, Degradation of aryl-azo-naphthol dyes by ultrasound, ozone and their combination: effect of R-substituents, Ultrason. Sonochem. 13 (2006) 208–214.

[32] K. Sahel, N. Perol, H. Chermette, C. Bordes, Z. Derriche, C. Guillard, Photocatalytic decolorization of Remazol Black 5 (RB5) and Procion Red MX-5B—isotherm of adsorption, kinetic of decolorization and mineralization, Appl. Catal. B: Environ. 77 (2007) 100–109.

[33] I. Poulios, I. Tsachpinis, Photodegradation of the textile dye Reactive Black 5 in the presence of semiconducting oxides, J. Chem. Technol. Biotechnol. 74 (1999) 349–357.

[34] N. Takeda, T. Torimoto, S. Sampath, S. Kuwabata, H. Yoneyama, Effect of inert supports for titanium dioxide loading on enhancement of photodecomposition rate of gaseous propionaldehyde, J. Phys. Chem. B 99 (1995) 9986–9991.

[35] A. Mills, R.H. Davis, D. Worsley, Water-prification by semiconductor photocatalysis Chem, Soc. Rev. 22 (1993) 417–425.

[36] J.-M. Herrmann, Heterogeneous photocatalysis: fundamentals and applications to the removal of various types of aqueous pollutants, Catal. Today 53 (1999) 115–129.

[37] J. Cunningham, G. Al-Sayyad, S. Srijaranai, Adsorption of model pollutants onto TiO2 particles in relation to photoremedation of contamined water, in: G. Helz, R. Zepp, D. Crosby, D. Lewis (Eds.), Aquatic and Surface Photochemistry, 22, CRC press, Boca Raton, Florida, 1994, pp. 317–348. Chapter 3.

[38] J. Cunningham, G.H. Al-Sayyed, Factors influencing efficiencies of TiO2-sensitised photodegradation. Part 1.—Substituted benzoic acids: discrepancies with dark-adsorption parameters, J. Chem. Soc. Faraday Trans. 86 (1990) 3935–3941.

[39] Y. Xu, C.H. Langford, Variation of Langmuir adsorption constant determined for TiO$_2$-photocatalyzed degradation of acetophenone under different light intensity, J. Photochem. Photobiol. A: Chem. 133 (2000) 67–71.

[40] C. Minero, A rigorous kinetic approach to model primary oxidative steps of photocatalytic degradations, Sol. Energy Mater. Sol. C 38 (1995) 421–430.

[41] G.T. Li, J.H. Qu, X.W. Zhang, H.J. Liu, H.N. Liu, Electrochemically assisted photocatalytic degradation of Orange. II. Influence of initial pH values., J. Mol. Catal. A 259 (2006) 238–244.

[42] S.Y. Yang, L.P. Lou, K. Wang, Y.X. Chen, Shift of initial mechanism in TiO$_2$-assisted photocatalytic process, Appl. Catal. A 301 (2006) 152–157.

[43] Y.X. Chen, S.Y. Yang, K. Wang, L.P. Lou, Surface characteristic in UV-illuminated photodegradation of Acid Orange 7, J. Photochem. Photobiol. A 172 (2005) 47–54.

[44] A.H. Nethercot, Prediction of fermi energies and photoelectric threshold based on electronegativity concepts, Phys. Rev. Lett. 33 (1974) 1088–1091.

[45] F. Hongbo, P. Chengshi, Y. Wenqing, Z. Yongfa, Visible-light-induced degradation of Rhodamine B by nanosized Bi$_2$WO$_6$, J. Phys. Chem. B 109 (2005) 22432–22439.

[46] Y. Kim, S.J. Atherton, E.S. Brigham, T.E. Mallouk, Sensitized layered metal oxide semiconductor particles for photochemical hydrogen evolution from nonsacrificial electron donors, J. Phys. Chem. B 97 (1993) 11802–11810.

[47] W.J. Li, D.Z. Li, W.J. Zhang, Y. Hu, Y.H. He, X.Z. Fu, Microwave synthesis of Zn$_x$Cd$_{1-x}$S nanorods and their photocatalytic activity under visible light, J. Phys. Chem. C 114 (2010) 2154–2159.

[48] A.J. Bard, R. Parsons, J. Jordan, Standard Potentials in Aqueous Solution, Marcel Dekker, New York, 1985.